WELDING RESEARCH

SUPPLEMENT TO THE *WELDING JOURNAL*, MARCH 1995
Sponsored by the American Welding Society and the Welding Research Council

Particulate-Reinforced Metal Matrix Composite as a Weld Deposit

A method for producing particulate-reinforced metal matrix composite weld metal is identified

BY E. I. KIVINEVA, D. L. OLSON AND D. K. MATLOCK

ABSTRACT. Weld metal consisting of particulate-reinforced metal matrix composite structure was produced with ceramic or refractory metal powder filled cored wire. Results are presented for both gas tungsten arc and gas metal arc weldments on Type 304 stainless steel. The effect of powder particle density and size distribution on the dispersion of particulates in the weld deposit was investigated. The motion and final distribution of particulates in the weld pool were evaluated with a fluid mechanics-based model, and critical welding criteria for the production of uniform particle distributions were identified. With particulates of optimum size and density in powder-filled cored wire it was possible to produce arc welding particulate-reinforced metal matrix weld deposits having uniform spatial particle distributions.

Introduction

Development of solidified weld metals with unique microstructures and properties continues to challenge welding engineers as materials with improved properties for more demanding applications are required. Significant advancements have been made in microstructural control by engineering specific combinations of joint geometry, alloy content and solidification structure. However, the potential exists for weld metals with superior properties if the principles which have been applied to engineer new materials, such as particulate-reinforced metal matrix composites (MMC), are applied to the development of weld metals. In this paper, the basics of the development of particulate-reinforced MMC weld metals for high-temperature applications are considered.

Metal matrix composites usually consist of dispersed high-strength fibers or particles in a continuous ductile phase. The composite properties depend on the volume fraction, morphology, and distribution of the second phase, and thus metal matrix composites offer the opportunity to engineer materials with specific properties. For example, the low-temperature strength of particulate-reinforced metal matrix composites increases with an increase in the volume fraction and strength of the particles (Ref. 1), while the high-temperature creep resistance increases with a decrease in interparticle spacing, as would be obtained at a constant volume fraction with a decrease in particle diameter (Refs. 2–5).

Fabrication of MMC materials requires the use of specialized processing techniques to produce materials with controlled uniform distributions of the second phase (Ref. 6). Fiber composites are often fabricated by laminating multiple layers of thin foils strengthened by single fiber layers, while particulate-reinforced metal matrix composites can be produced by mechanically working sintered powder metallurgy compacts, infiltration techniques, or semisolid metal forming. In general, it is anticipated that production of particulate-reinforced metal matrix composites directly in solidified microstructures would be difficult, as on solidification insoluble second phase particles would be rejected to the liquid and would be either trapped in

KEY WORDS

Particulate MMC
Weld Deposit
Cored Wire
Composite Consumable
Particle Distribution
Ceramic Powder
Refractory Metals
Particle Transfer
Hardness Profile
Metallography

E. I. KIVINEVA is with Lokomo Oy Lokomo Steels, Tampere, Finland. D. L. OLSON and D. K. MATLOCK are with Center for Welding and Joining Research, Colorado School of Mines, Golden, Colo.

Table 1 — Physical Properties of the Welding Wire Matrix and Powder Materials (Refs. 20, 21)

Material	Density (kg/m³)	Melting Temperature (°C)	Hardness[a]
AISI 310	8000	1400	150
Tungsten	19300	3410	450
Tungsten carbide	25600	2870	3000
Niobium carbide	7600	3500	2470
Titanium carbide	4900	3140	3200

(a) Converted to Vickers hardness.
The hardness values of the powder materials are microhardness values expressed in Vickers hardness numbers.

the final liquid to solidify or would be removed in the slag on the surface of the solidified material. However, in contrast to solidification in normal castings, the high solidification rates and inherent weld bead stirring associated with welding offer control variables, which may be utilized to entrap a fine distribution of particles in solidified weld metal.

Similar interests in producing weld deposits that contain a high particulate content have been investigated by researchers (Refs. 7–11) interested in hard surfacing and in the welding of metal matrix composites. Lugscheider (Ref. 7) investigated the behavior of various carbides during plasma arc surfacing. Hard cobalt weld deposits were made with hard carbide materials (WC, TiC, (W,Ti)C, NbC or VC) and interactions, such as the dissolution tendency of the various carbides between the alloy and the carbide were characterized. The deposit properties were correlated to the nature of these carbides.

Welding of particle-reinforced SiC/Al weld matrix composite has been investigated (Refs. 8, 10). The solidification of autogenous laser welds has been characterized and modeled (Ref. 8). GMA welding of Al-Al_2O_3 metal matrix composite using conventional aluminum welding consumables has been performed to evaluate the particle incorporation in the weld deposit (Ref. 9). The fusion welding of SiC-reinforced aluminum alloys has also been investigated (Refs. 10, 11).

One application for particulate-reinforced weld deposits would be in welded assemblies for high-temperature service. Stainless steel weld metals exhibit shorter creep lives than those with similar wrought compositions during high-temperature service (Ref. 12). Hard, fine insoluble second phase particulates with a uniform spatial distribution in the weld metal can act as obstacles against dislocation movement and increase the creep life (Ref. 2). Wilshire, *et al.* (Refs. 3, 13), demonstrated that with dispersed second phase particles of the proper size, the creep rate can be decreased by an order of magnitude.

The purpose of this paper is to investigate the fundamental issues associated with the production of metal matrix composite weld metals by direct transfer of particulates from the welding consumables to a molten weld pool.

Particulate second phase particles in stainless steel weld metal are considered. Several fundamental questions are evaluated in this study:

1) What type of particulates can be used and how can they be effectively transferred through the arc?

2) What influence does the particle type, size variation, and density have on the transfer loss and distribution uniformity?

3) What is the nature of particulate-reinforced MMC weld deposit?

4) How would particulate-reinforced MMC consumables be made?

5) Is it possible to produce sufficiently fine particles needed to increase creep life and survive the arc welding process?

6) What design rules would be necessary to produce MMC consumables for desired properties?

The ability to produce solidified particulate-reinforced MMC weld metal will depend on the behavior of the particles in the liquid pool and during solidification. After transfer from the welding consumable there are five primary responses that can be exhibited by the particles in the liquid pool: 1) they can dissolve; 2) float to the top of the pool; 3) sink to the bottom of the pool; 4) remain suspended and be rejected to the liquid during solidification; or 5) remain suspended and be entrapped in the solid by the advancing solidification front. The response of a particular particle type depends on the particle density, solubility, and size distribution in conjunction with the solidification rate. In the following sections the fundamental principles related to the interaction of particles with a moving solidification front and the migration of particles in a liquid are considered.

Table 2 — Summary of Particle Size Distributions

Powder	Sieve Analysis	Particle Size, μm
Tungsten—uncoated		Average size, 0.5
Tungsten—uncoated	−100 mesh	<149
Tungsten + sol-gel coating	−325 + 500 mesh	25 to 44
Tungsten + sol-gel coating	−200 + 325 mesh	44 to 74
Tungsten + sol-gel coating	−100 to 200 mesh	74 to 140
Tungsten + sol-gel coating	−60 + 100 mesh	140 to 250
Tungsten carbide		Average size 1
Niobium carbide		Average size 2
Titanium carbide		Average size 0.5

Solidification of Weld Metal with Insoluble Particulates

The distribution of particles in metal matrix composites manufactured by a solidification process depends on the nature of the interaction between the particles and the growing solidification front. When a moving solidification front intercepts an insoluble particle, the particle can be either pushed ahead of the front or engulfed within the solidified microstructure. Engulfment occurs through growth of the solid over the particle, followed by enclosure of the particle in the solid (Ref. 14).

A thermodynamic model suggested by Omenyi and Neumann (Ref. 15) predicts engulfment when the net change in free energy due to engulfment is negative. A model proposed by Uhlmann, *et al.* (Ref. 16), documented the existence of a critical interface velocity, V_{cr}, of the solidification front. Below the critical velocity, particles are rejected to the liquid ahead of the solidification front, while above the critical velocity, the particles are continually engulfed in the solidified metal. The critical velocity, V_{cr}, has been experimentally found (Ref. 17) to depend on particle radius, r_p, according to the following relationship:

$$V_{cr}\, r_p^{\,n} = \text{constant} \qquad (1)$$

where the exponent n ranges from 0.28 to 0.90 depending on the material system.

Other independent physical variables affecting particle behavior at the melt interface are: viscosity of the liquid (η), interfacial energies, (σ_{PL}, σ_{PS} and σ_{LS}), particle shape and density of liquid (ρ_L). Particle aggregation, particle shape, and particle density (ρ_P) must be controlled

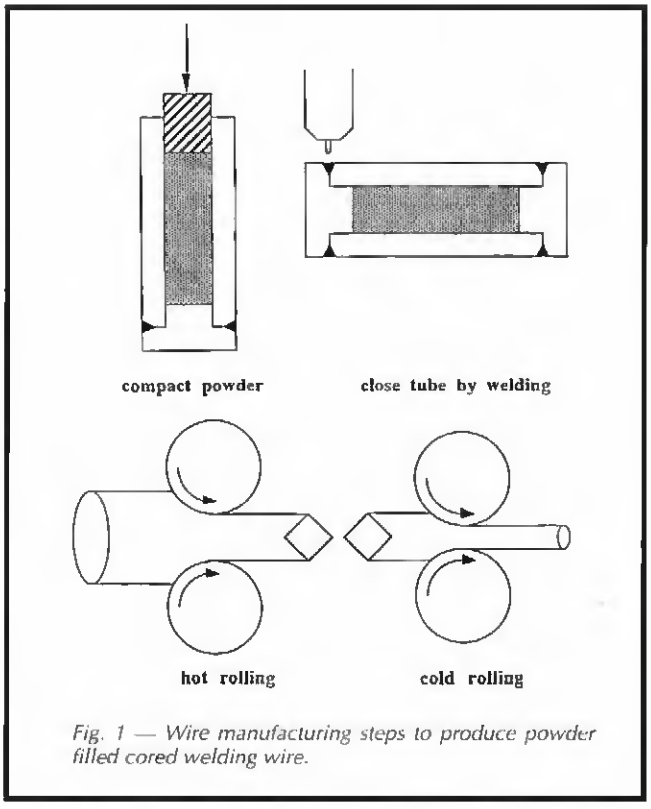

Fig. 1 — Wire manufacturing steps to produce powder filled cored welding wire.

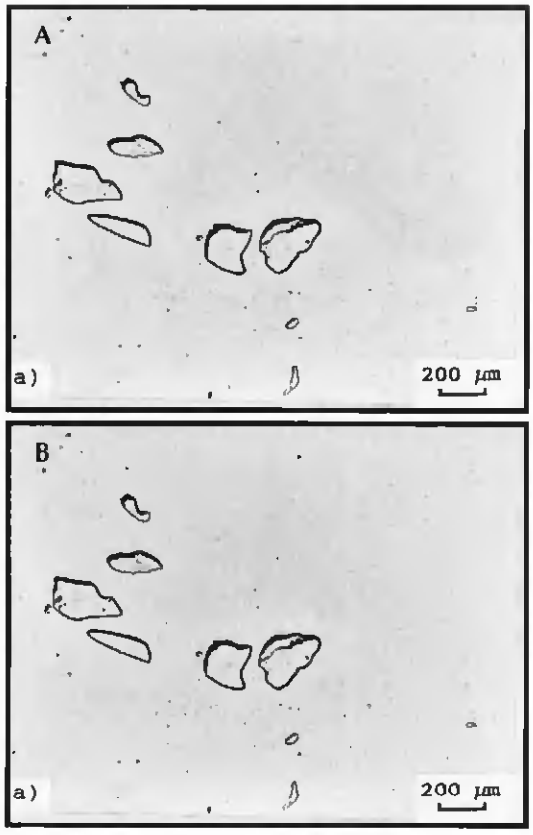

Fig. 2 — The microstructure of uncoated –100-mesh tungsten powder cored filler metal gas metal arc welds. A — weld center; B — lower weld.

(Ref. 17). In the experimental program outlined below, η, and ρ_L are assumed constant for stainless steel, and σ_{PL}, σ_{PS}, and σ_{LS} are assumed constant for a specific particle type in the stainless steel matrix. The remainder of the variables are considered in the experimental matrix.

Movement of Insoluble Particles in Liquid Media

The motion of particulates in the weld pool can be modeled using fluid mechanics with a knowledge of the relative densities of the liquid and the particles and the average particle size. For a particle in liquid metal, the force balance which considers the buoyancy force, the friction force (*i.e.*, drag in the liquid), and the gravitational force can be expressed as (Ref. 18):

$$\frac{4}{3}\pi r_p^3 \rho_L g + 6\pi\eta r_p V_L = \frac{4}{3}\pi r_p^3 \rho_p g \quad (2)$$

where V_L is the velocity of the liquid and g is the acceleration due to gravity.

There are two conditions where a spherical particle with radius r_p will be suspended or where Equation 2 holds. The first condition is where V_L is in the direction of gravity ($V_L>0$) and the density of the particle ρ_P is greater than the density of the liquid, ρ_L. The second condition is where V_L is in the direction opposite of the direction of gravity ($V_L<0$) and the particle density is less than the density of the liquid (Ref. 19). In a stirred weld pool, both velocity vector directions are experienced. These two conditions can be described by Equation 3.

$$V_L = \frac{2 r_p^2 (\rho_p - \rho_L) g}{9\eta} \quad (3)$$

When the magnitude of the velocity of the weld pool is greater than the calculated suspension velocity, the analysis suggests that the particles will go with the stream and particle dispersion is expected. If the magnitude of the weld pool velocity is less than this suspension velocity, the particulates will sink or float depending on their density, and dispersion is not expected. When the particles do not disperse, there is a greater probability for interaction and agglomeration.

Experimental Design

The theoretical discussion above indicates that four primary variables must be considered to determine the potential for producing particulate-strengthened metal matrix composite weld metal: particle buoyancy as controlled by particle density and size, particle drag as controlled by particle size and liquid viscosity, particle dissolution rate as controlled by the type of particle and liquid matrix, and solidification rate as controlled by the welding process.

Experimental weldments were produced by both gas tungsten arc and gas metal arc welding processes on AISI 304 stainless steel plate with cored welding wires produced from AISI 310 stainless steel tubing. AISI 310 stainless steel was chosen to be representative of creep-resistant stainless steel alloys and to provide a weld pool that solidified with a fully austenitic structure. The two welding processes were chosen to produce two significantly different solidification rates and modes of transfer of the particulate into the pool.

Powders were chosen to represent significant variations in density and thermodynamic stability. Pure tungsten powders were evaluated in two conditions: as-received and as-modified with a sol-gel coating. The sol-gel coating is a glass coating which decreased the dissolution rate. In addition, carbide particles of tita-

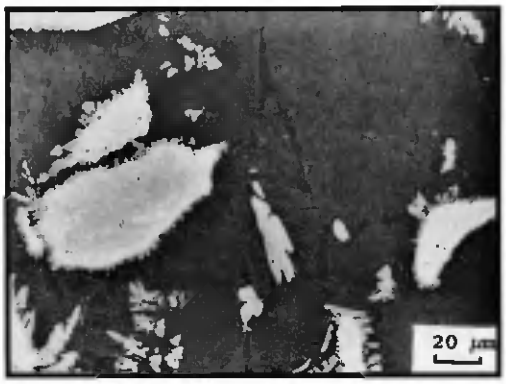

Fig. 3 — SEM micrograph of uncoated –100 mesh tungsten powder cored filler metal gas tungsten arc weld showing an intermetallic zone at the powder-matrix interface.

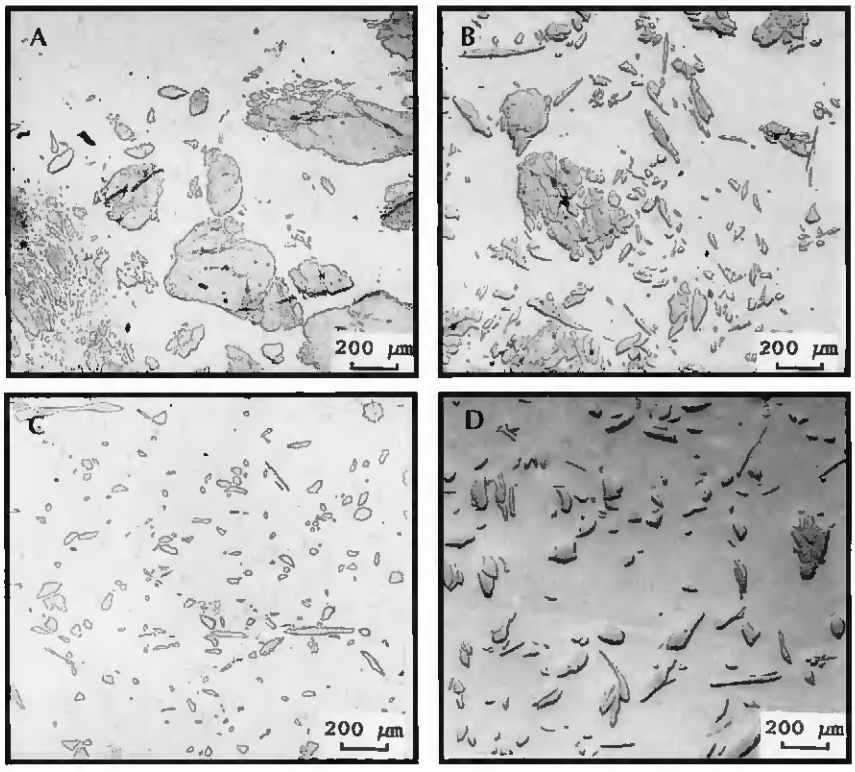

Fig. 4 — The microstructure of glass coated tungsten powder cored filler metal GTA weld deposits. The micrographs are for the weld center location for various powder sizes: A — –325+500 mesh; B — –200+325 mesh; C — –100+200 mesh; D — –60+100 mesh.

nium, niobium, and tungsten were evaluated to determine the effect of density. Particle size distribution was evaluated with the sol-gel coated tungsten powders.

Experimental Procedure

Powder Materials

The distributed second phase was added to the weld deposit by the introduction of tungsten powder, tungsten carbide, niobium carbide and titanium carbide powders from a tubular consumable during the arc welding process. The powder materials were chosen based on the requirement that their hardnesses and melting temperatures would be higher than those of AISI 310 stainless steel. The densities of the powders varied from 5000 to 19,000 kg/m^3, while the density of AISI 310 stainless steel was approximately 8000 kg/m^3. The density, melting point, and room-temperature hardness of the matrix and the powder materials are presented in Table 1. All of the powders exhibited melting points significantly greater than the AISI 310 stainless steel. The density of niobium carbide was essentially the same as the stainless steel, while the densities of tungsten and tungsten carbide were significantly greater, and the density of titanium carbide was significantly less.

The experimental powder particle sizes are summarized in Table 2. Two commercial uncoated tungsten powders, a "fine" powder with an average particle size of 0.5 μm and a coarse, –100-mesh powder with a maximum particle size of 149 μm, were obtained to evaluate the effects of average particle size. In addition, the coarse powder was put through a sieve set to produce additional materials with controlled size ranges for coating by the sol-gel process discussed below. The tungsten carbide, niobium carbide and titanium carbide powders were each obtained with single average particle sizes of 1, 2 and 0.5 μm, respectively.

Sol-Gel Coating Process

The sol-gel process (Ref. 22) was used to produce a SiO_2 glass coating on the surface of each particle in sets of sized tungsten powders. The particle size ranges are indicated in Table 2. The glass coating was produced by mixing wet tungsten powder with tetraethyl orthosilicate (TEOS), $Si(C_2H_5O)_4$. Moisture on the particulates reacted with TEOS and a glass coating was formed on the surface of each particle. The specific chemical reaction sequence is as follows. TEOS reacts with water to produce a solution of $Si(C_2H_5O)_3OH$ and ethanol, C_2H_5OH. If water is present, polymerization takes place and $Si(OH)_4$ forms a gel. With the wet particle, this process occurs at the particle surface to produce a coating. After the sol-gel coating process, the powder was dried in a furnace at 350°C (662°F) in an argon gas atmosphere.

Cored Wire Fabrication

The experimental cored welding wires were fabricated from AISI 310 stainless steel tubing using procedures developed previously (Ref. 23). The wire was produced from 200-mm (8-in.) long AISI 310 stainless steel tubing with 25-mm (1-in.) outer diameter and 5.5-mm (0.22-in.) wall thickness. The powder was packed in the tube with a hydraulic press using 53 kN packing force to produce a compact with approximately 17.5 vol-% powder (a density which was calculated assuming a packing efficiency of approximately 50%.) After packing, end caps were welded on each tube, and the tubes were hot rolled to 5-mm (0.20-in.) diameter rod and cold rolled to the final

Table 3 — Gas Tungsten (GTAW) and Gas Metal Arc Welding (GMAW) Parameters Used to Produce Particulate Composite Weld Deposits

Welding Process	Current (A)	Voltage (V)	Wire Feed (mm/s)	Torch Speed (mm/s)	Estimated Heat Input KJ/mm
GTAW	200 A	12 V	Manual	Manual 0.5[a]	4.8
GMAW	300 A	25 V	58	3.3	2.3

(a) Estimated.

diameter of 2.5 mm (0.10-in.) on a laboratory rolling mill equipped with rod rolls. The manufacturing sequence is illustrated schematically in Fig. 1. The wire surface was cleaned mechanically using a wire brush and by grinding to remove the oxide layer and any flash from the rolling process. This practice produced approximately 20 m (65.6 ft) of welding wire for each powder addition.

Welding Procedure

Single-pass weld deposits were made on a 12.5-mm (0.5-in.) thick AISI 304 stainless steel plate in a single V-groove with 90-deg included angle, and a 1-mm load. Both gas tungsten arc (GTA) and gas metal arc (GMA) welding procedures were used. GTA welding of the test materials was done using a 3-mm (0.12-in.) diameter tungsten welding electrode, an argon shielding gas, and direct current electrode negative. Weld deposits were produced by manually feeding into the weld pool. The GMA welding procedure used an automatic torch carriage assembly with argon shielding gas. The GMA welds were made using direct current electrode positive polarity. The welding parameters for each process are summarized in Table 3. Qualitatively, the welding conditions resulted in the GMA weld having a greater solidification rate than the GTA weld. Selected welds were also produced with alternating and pulsation current modes with the GTA welding process to study the effect of the welding current mode on the dispersion and recovery of particles in the weld pool.

Metallography and Hardness Testing

Welded samples were ground, polished and examined with light microscopy. The area fraction measurements and size distributions of the second phase particles were determined with an optical image analyzer. A scanning electron microscope (SEM) with an energy dispersive spectrometer (EDS) was used to study the dissolution of the powder materials in the weld metal. Microhardness values of the weld deposits were determined as a function of position across the weld pool with a 500-g test load.

Results

The results consisted primarily of micrographs from the weld deposits made with the experimental powder-filled cored welding wires. The effects of particle type, size, and size distribution on the weld metal microstructures were evalu-

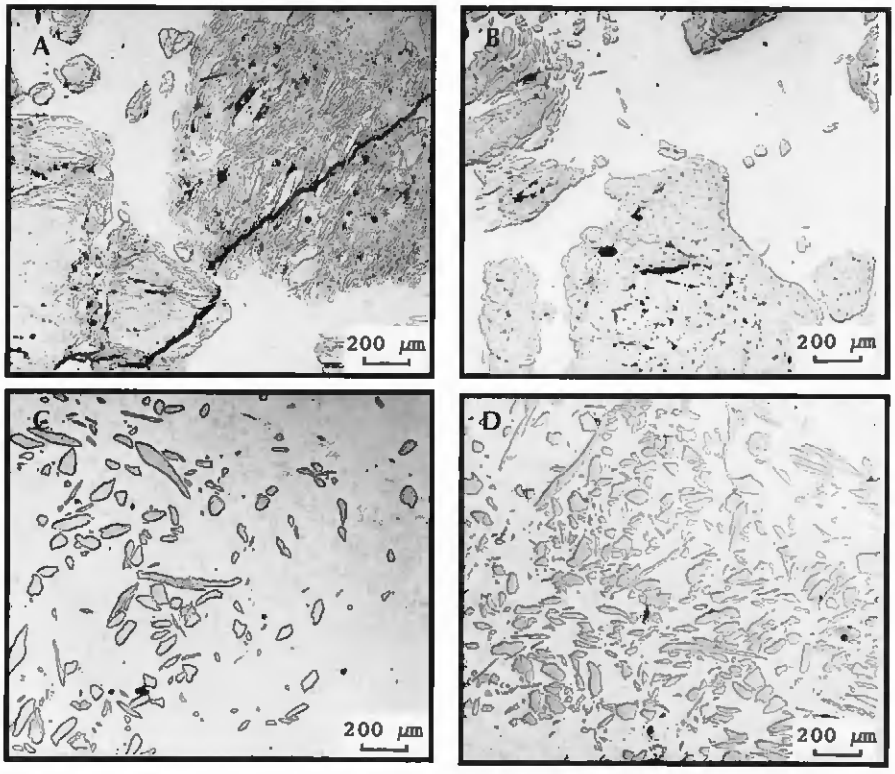

Fig. 5 — The microstructure of glass coated tungsten powder cored filler GTA weld deposits. The micrographs are for the lower weld location for various powder sizes: A — –325+500 mesh; B — –20O+325 mesh; C — –100+200 mesh; D — –60+100 mesh.

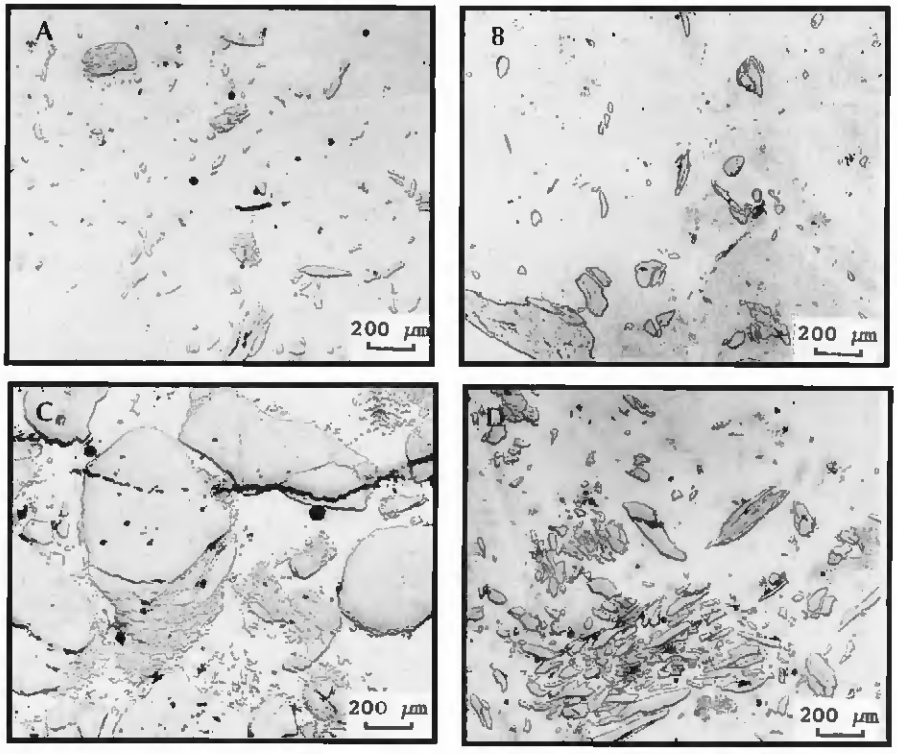

Fig. 6 — The microstructure of glass coated tungsten powder cored filler GMA weld deposits: A — weld center location for –200+325 mesh; B — weld center location for –60+100 mesh; C — lower weld location for –200+325 mesh; D — lower weld location for –60+100 mesh.

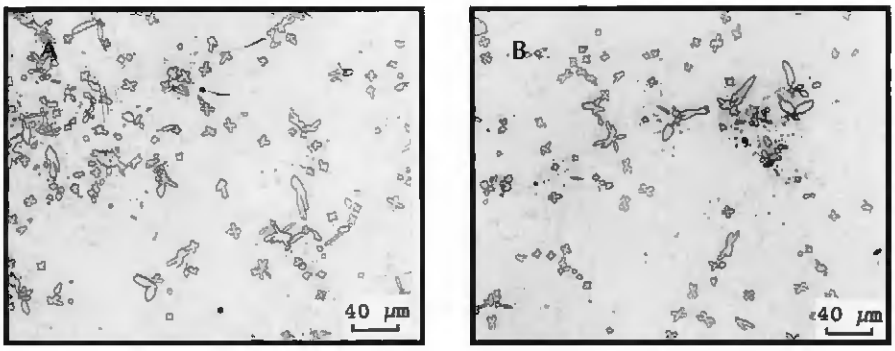

Fig. 7 — The microstructure of a 2.0 μm niobium carbide powder cored wire GMA weld deposit. A — Weld center; B — lower weld.

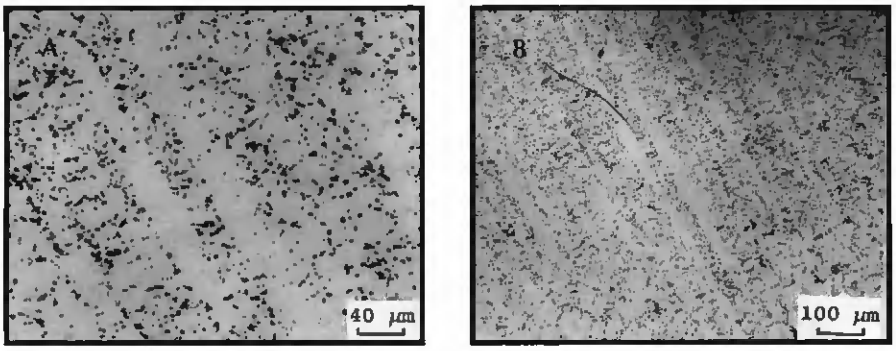

Fig. 8 — The microstructure of 0.5 μm titanium carbide powder cored wire GTA weld deposit. A — High magnification; B — low magnification of the same area.

ated and compared. For each weld, micrographs were obtained as viewed parallel to the welding direction at three locations: just below the external surface at the top of the weld, at the midpoint or the center of the weld, and in the weld root just above the fusion line at the bottom of the weld. The observations for each particle type were first analyzed and then the results were compared to develop a predictive procedure for the development of particulate-reinforced MMC weld metal.

Tungsten Powder — Uncoated

Uncoated tungsten powders with 0.5 μm and 100 mesh (<149 μm) particle sizes were investigated with both GMA and GTA welding processes and the observations were similar for both. Significant dissolution occurred, and as a result, a limited number of particles was entrapped in the matrix. A large amount of the powder was found on the surface of the weld pool after solidification and some of the powder was assumed to vaporize during metal transfer through the welding arc. The remaining undissolved powder agglomerated and was mostly found in the bottom of the weld pool. Representative light micrographs, which show the particle size dependence of the weld center and weld root microstructures, are shown in Fig. 2 for a GMA weld. Random particles were observed in the weld center, and particle agglomeration is evident at the weld root. The particles that are greater than 149 μm represent particles which agglomerated either during wire manufacture or the welding process.

Pulsed GTA and alternating current GTA welding procedures were used to study the effect of arc current mode on the powder dispersion in the weld pool. Neither method was found to reduce clustering with uncoated tungsten powder welding wire. During pulsed current and alternating current GTA welding, the amount of tungsten that had dissolved in the matrix was measured to be higher than with direct current GTA welding.

The reactivity of the pure tungsten particles is illustrated in Fig. 3, which shows a SEM micrograph of tungsten particles within a GTA weld. An intermetallic reaction layer on the surface of each particle is evident. Based on SEM/EDS analysis, the composition of this layer was shown to be similar to the reaction zone layer in tungsten reinforced iron-based alloys reported by Claufield, *et al.* (Ref. 24), and was enriched with tungsten, iron and chromium.

Tungsten Powder — Glass-Coated by the Sol-Gel Process

Tungsten powders with four particle size distributions were treated by a sol-gel process to produce a glass coating on each particle. The coating was added to produce a physical barrier to minimize losses due to particle dissolution, and thus, to enhance the amount of the second phase particles entrapped in the weld metal.

The effects of sol-gel coating and particle size on GTA weld metal microstructures are shown in Figs. 4 and 5. Figure 4 presents the weld center microstructures and Fig. 5 presents the corresponding weld root microstructures. As shown in Fig. 4A for the finest powder, significant agglomeration occurred. However, with an increase in particle size, the particle distribution was more dispersed as shown in Fig. 4C and 4D. Similar changes in the particle distribution were observed in the weld root microstructures shown in Fig. 5 except that for each powder, the volume fraction of second phase was significantly higher at the bottom of each weld.

Figure 6 presents corresponding weld metal microstructures for two gas metal arc welds. Figure 6A and 6B, respectively, shows the weld center microstructures for a fine (–200+325 mesh) and coarse (–60+100 mesh) particle size. The corresponding weld root microstructures are shown in Fig. 6C and 6D. In comparison to the GMA welds in Fig. 6, as shown in Fig. 5, the GTA welds produced a slightly more uniform particle dispersion, a difference that is attributed to difference in cooling rates.

In the weld deposits produced with coated tungsten powders, particle recovery was better than for welds produced with the uncoated tungsten powder. Intermetallic phases were observed in the welds produced with coated tungsten powder, but the reaction layer that had been observed in the uncoated tungsten powder weld metal interface was smaller in the weld deposit with coated powder. This observation indicates that the dissolution rate was reduced with coated powder but not completely suppressed.

Tungsten Carbide Powder

Tungsten carbide was selected for a powder material to represent a potential second phase material with density between the densities of tungsten and the stainless steel matrix. The experiments with tungsten carbide powder filled cored wire using both gas metal arc and gas tungsten arc welding procedures

showed poor recovery of second phase particulates in the weld pool, and as a result, no micrographs are presented here. A large fraction of the powder chemically dissociated in the arc or dissolved in the matrix. The rest of the powder formed large clusters located in the bottom of the welds. Solidification cracking was observed in the weld metal around the powder agglomerates. The cracks were detected in both GMA and GTA welded deposits.

Niobium Carbide Powder

Niobium carbide, which has a density just below that of stainless steel, was used to study the solidification behavior of composite weldments when the densities of the components were similar. The GMA weld center and weld root microstructures are shown in Fig. 7. In contrast to the welds considered above, the GMA weld exhibited uniform particle distribution throughout the weld bead. Some clustering of the powder was detected, but the agglomerates were smaller than those in GTA welded deposits with niobium carbide particle powder. No solidification cracking was observed in the weld metal produced with niobium carbide filled wire.

In the micrographs shown in Fig. 7, cross-shaped particles were observed. The presence of these particles indicated that particle dissolution occurred with a preferred orientation. Reaction zones, as observed with the tungsten and tungsten carbide particles, were not observed at the particle-matrix interface for the niobium carbide particles. Chemical analysis indicated that even though there was evidence of some dissolution, the rate of dissolution was low as there was a limited increase in the niobium concentration within the weld metal matrix.

Titanium Carbide Powder

Titanium carbide, which had the lowest density of the test material powders, was selected to study weld deposit solidification with low density powder particles. The weld center and weld root microstructures for the GTA weld are shown in Fig. 8 and for the GMA weld in Fig. 9. For both welding processes, the particle distributions were essentially uniform. However, a comparison of Figs. 8A and 9A indicates that the cooling rate, as controlled by the welding process, altered slightly the particle distribution as seen by the dendritic solidification structure in Fig. 8A. Titanium carbide particles were rejected to interdendritic areas during solidification of GTA welded deposits so

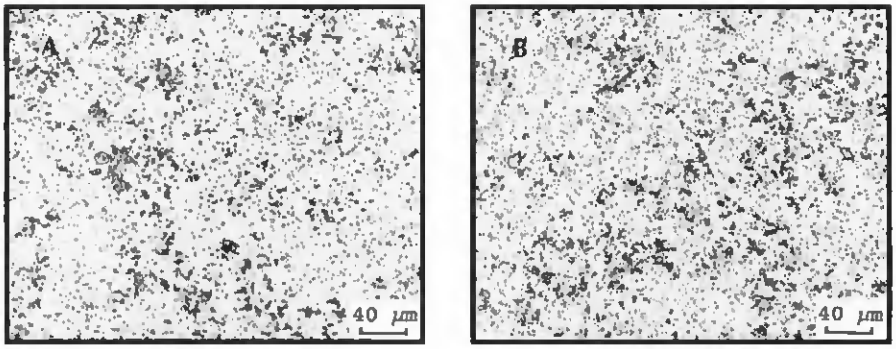

Fig. 9 — The microstructure of 0.5 μm titanium carbide powder cored wire GMA weld deposit. A — Weld center; B — lower weld.

that the dendrite arms could be observed in the solidification structure. This observation did follow the behavior suggested in Equation 1. From a comparison of Figs. 8 and 9, GTA welding appeared to result in a slower solidification velocity in comparison to GMA welding. In Equation 1, it was indicated that the interface velocity during solidification had a critical value of V_{cr}. Below this velocity, the particles were pushed into last solidifying areas. In the GMA weld deposit shown in Fig. 9, the particles were not found primarily in the interdendritic areas as they were in GTA weld deposit presented in Fig. 8. The difference in particle distribution was interpreted to occur because of the difference in the cooling rate of the weld pool as a result of the different welding procedure used.

Chemical analysis indicated that the dissolution rate of the powder in the matrix was low and acceptable. The dissolution rate of titanium carbide in the matrix was the lowest among the test materials that were used. No reaction zone around the TiC particles was detected. Cracking did not occur in the weld pool produced with titanium carbide powder-filled wire. The TiC particulate-austenite matrix combination with the proper particle size showed promise as particulate-reinforced MMC weld deposit material.

Hardness Profiles

The effects of the various particles on the mechanical properties of the weld deposits were evaluated with hardness

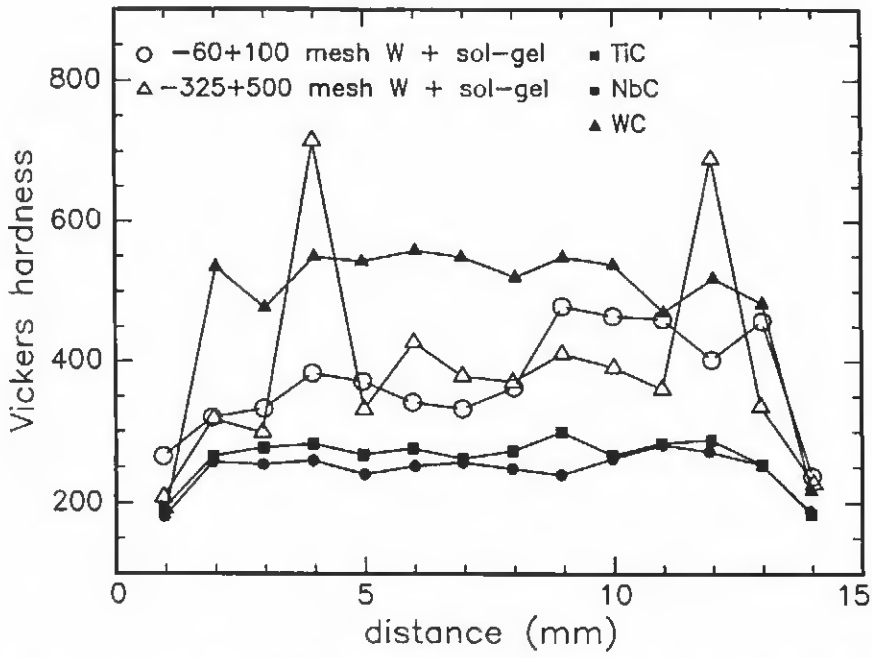

Fig. 10 — Transverse microhardness profiles of the GMA composite weld deposits. The profiles traverse across the weld beads from fusion line to fusion line.

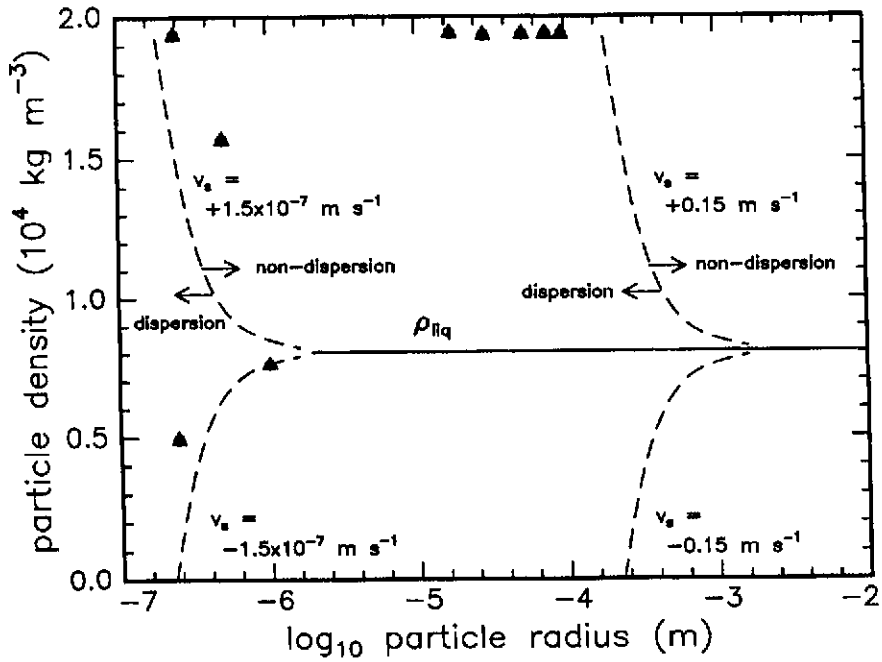

Fig. 11 — Particle density/particle radius map which identifies regions of nondispersion and dispersion during weld metal solidification at two different weld pool fluid velocities: $v_s = 1.5 \times 10^{-7}$ m/s and $v_s = 0.15$ m/s. The data points indicated on the map plot the particle density/particle radius combinations for the experimental materials of this study.

data. The weld metal hardness was measured with microhardness readings spaced 1 mm across the weld. These measurements were taken to determine the effect of possible dissolution of powder particles on the hardness and the results for GMA welds are shown in Fig. 10. Figure 10 shows that the average hardness values of weld metal produced with tungsten carbide powder-filled cored wire were the highest of the materials investigated. This result occurred because of the high-dissolution rate of the tungsten carbide powder during the welding procedure.

High-hardness peak values in the weld metal produced with –325+500 mesh tungsten filled powder were caused by the powder clusters in the weld deposit. The hardness values of weld deposits with titanium carbide and niobium carbide were measured to be the lowest among the test materials. This result may indicate that the dissolution rate of these powder materials in the weld deposit was the lowest.

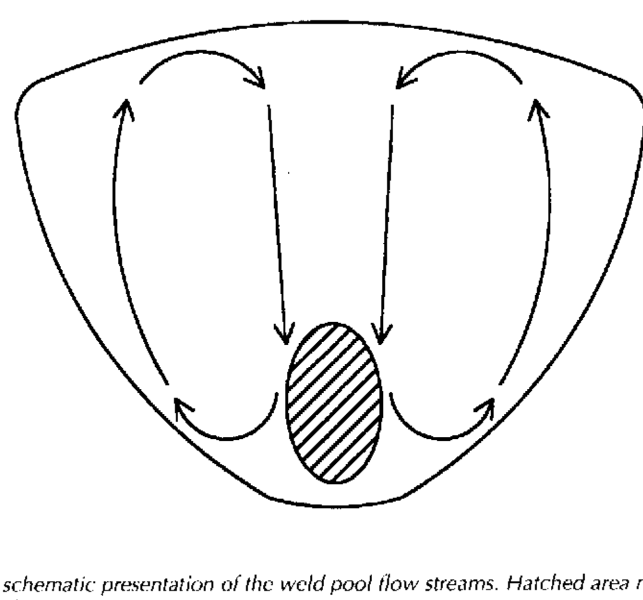

Fig. 12 — A schematic presentation of the weld pool flow streams. Hatched area marks the area with $v_s \approx 0$ m/s.

Discussion

Movement of the Particles in the Liquid Weld Metal

Based on a force balance for two special conditions (Equation 3), and an assumed weld pool velocity, V_{wp}, the relationship between particle density and particle radius was used to calculate the boundary line between particle agglomeration tendency and particle distribution tendency. Calculations were made with a liquid metal viscosity (η) of 0.006 kg/Ms (Ref. 25). In Fig. 11 boundary lines between suspension and agglomeration were plotted as a function of particle radius and density for two assumed weld pool velocities, 0.15 m/s and 1.5×10^{-7} m/s. The assumed weld pool velocity of 0.15 m/s is typical for GMA and GTA welding (Ref. 26). In these calculations, the force balance conditions change depending upon whether the density of the particle is greater or less than the density of the liquid and the direction of the fluid flow. Figure 11 also plots the specific properties of the investigated powder materials. The curves above and below the density of the liquid metal (8000 kg/mm^3) represent the two possible conditions, described earlier, for a force balance on the particle in the liquid. Based on the concepts of this simplified model, the particles that are located to the right of a given velocity criteria curve would not disperse. It should be noted that this model ignores many of the complex particle-fluid-solidification interactions in a weld pool but still provides meaningful insight into the overall behavior.

All of the investigated powder materials are located to the left of the boundary curve for the 0.15 m/s weld pool velocity. However, nondispersion behavior was observed with some of the powder materials. This behavior was assumed to occur because the model does not take into account the powder interactions and because the flow conditions in the weld pool are more complicated than assumed in the model. The particle interactions are increasingly likely to occur with small powder size because the mean particle separation becomes smaller when the powder size is reduced with a constant powder volume fraction. This situation enhances the probability for interaction. Also, when powder particles have interacted and agglomerated, the effective particle size is increased. The particle size distribution can cause a

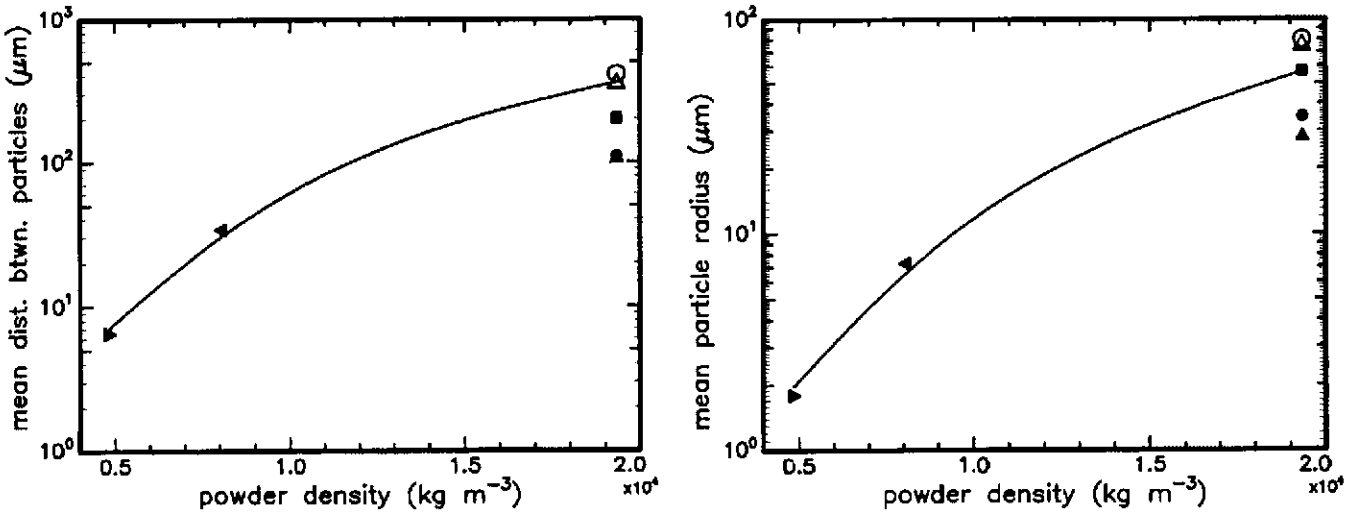

Fig. 13 — The mean particle radius (r) produced and mean distance between particles (λ) with different powder materials: ▶ TiC; ◀ NbC; ▲ 60+100 mesh + sol gel W; • 100+200 mesh + sol gel W; ■ 200+325 mesh + sol gel W; Δ –100 mesh uncoated W; and o –325+500 mesh + sol gel W.

difference between predicted and actual particle dispersion.

The liquid flow conditions are commonly presented schematically as in Fig. 12. The hatched area in the bottom of the weld pool in the figure illustrates an area where flow velocities are low. The low velocity area exists in the pool because these areas get trapped between streams. If the weld pool velocity, V, is low enough, it can cause a significant change in the particle density-particle size diagrams (Fig. 11). This condition can promote the interaction between powder particles and causes nondispersion of the particles and can lead to formation of agglomerates. In the area with low flow velocity, the probability for particle interaction and agglomeration is higher. The powder clusters that were found in the weld deposits produced with small particle size tungsten and tungsten carbide powders were located mainly in lower weld pool areas.

In Fig. 11 the effect of low weld pool velocity on the liquid velocity for particle suspension has also been illustrated by the dashed lines. In the figure it can be seen that if the weld pool velocity is 1.5 x 10^{-7} m/s only two of the experimental powders with densities 4900 and 7600 kg/m^3 would disperse. This result is consistent with the experimental observations.

Characterization of Particulate-Reinforced MMC Weld Deposit

The values for mean radius (r) and mean distance between particles (λ) were calculated from the image analyzer measurements and are shown in Fig. 13. The measurements showed that titanium carbide produced the smallest and niobium carbide the second-smallest average particle radius in the weld deposit. Measurements for weld deposits produced with wire filled with different tungsten powder sizes showed that the two initially largest size powders produced the smallest second phase particle radius for this set. This behavior occurred because the particles in weld deposits produced with a wire filled with small particle size powder tended to form large agglomerates in the structure. The formation of these agglomerates increased the effective particle radius. Figure 13 correlates particle size distribution and interparticle spacings with powder density. Such correlations are necessary in order to design creep resistant composite weld metal.

Conceptual Design Criteria of Composite Weld Deposits with Desired Properties

The design of particulate-reinforced MMC weld deposits must consider the

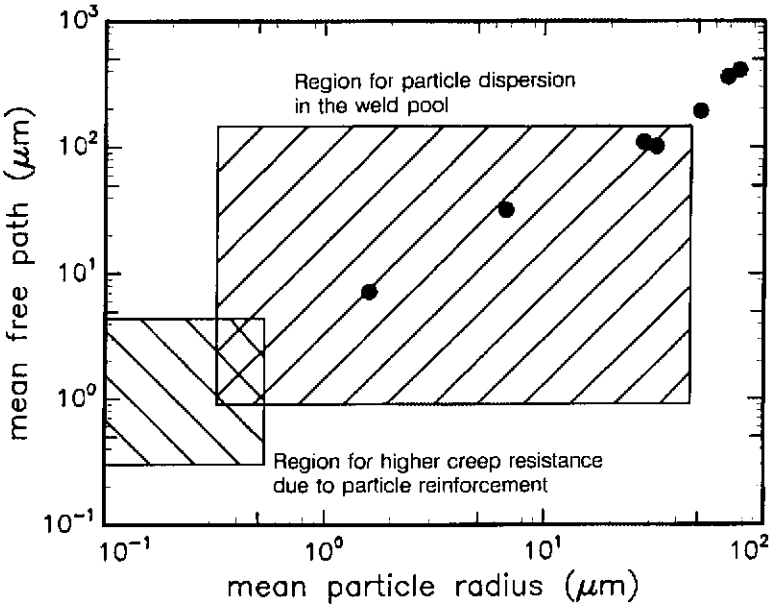

Fig. 14 — Conceptual design criteria for the particulate composite weld deposit indicating the region for particle distribution resulting from welding with particulate-filled cored wire and the region for enhanced creep resistance. The overlap defines the optimal conditions. The data points indicate the particle size and mean free path for weld deposits produced in this investigation.

criteria for enhanced creep resistance due to the particle reinforcement of the alloy and the effect of powder size distribution on the achieved microstructure. In Fig. 14 mean free path between particles was plotted as a function of mean particle radius for each experimental material. In addition, regions for particle dispersion in the weld pool and high creep resistance of particle-reinforced materials are identified. The higher creep resistance region is based on the relationship between mean particle radius and mean free path with fixed second phase percentage (Ref. 2). The particle reinforcement region ranges from 0.3 to 4.5 μm with an assumed 17.5 vol-% of second phase and particle diameter from 0.1 to 1 μm. The region which is marked as dispersion of particles in Fig. 14 is based on the observations in the experiments with different powder size distributions.

The optimum design criteria would be the overlapping area of these two regions in Fig. 14. In this area both the particle strengthening and the right processing conditions would be expected to coexist. Figure 14 therefore can be viewed as a design diagram to produce particulate-reinforced MMC welding consumables.

Conclusions

The research has demonstrated that particulate-reinforced MMC metal matrix composite weld deposits can be made and that the particles can be transferred through the arc into the weld pool. The efficiency of transferring particles depends on the composition and size of the powder. Transfer loss has been observed to be higher with smaller particle size with the same powder material.

Powder type and composition are important factors affecting the behavior of the second phase particles in the weld metal solidification structure. The powder should be chosen so that the expected reactions with the matrix material will be minimized. Coating can be used to slow down or prevent reaction, including dissolution, between particle and matrix.

Particle size is an important factor. This investigation has shown that particle size will influence the distribution of the particles in the weld pool together with the density of the powder. A uniform particle distribution can he reached with proper selection of matrix and powders and processing parameters. The criterion for optimum powder material include particle size, type, density and composition. Selection of welding process and welding variables will also influence particle distribution. Based on these results, the methodology for developing consumable design rules to achieve optimum weld deposit properties and processing conditions were presented.

Particulate-reinforced MMC consumables can be made with the same methods as flux cored welding consumables. In this study cold rolling was found preferable for manufacturing the particulate-reinforced MMC wire to drawing. As a proposed future improvement for making particulate-reinforced MMC weld deposits, it is suggested that different methods be explored to produce the powder filled cored welding wire.

Acknowledgments

The authors acknowledge and appreciate the support of the Basic Energy Science Division of the U.S. Department of Energy and Teledyne Wah Chang for providing test materials.

References

1. Frommeyer, G. 1983. Metallic composite materials. *Physical Metallurgy*, R. W. Cahn and P. Haasen, editors, Chapter 29, Elsevier Science Publisher, New York, N.Y.

2. Zhu, Z. G., and Weng, G. J. 1989. Creep deformation of particle-strengthened metal matrix composites. *J. Engineering Materials and Technology*, iil, pp. 99–105.

3. Threadgill, P. L., and Wilshire, B. 1974. The effect of particle size and spacing on creep of two-phase copper-cobalt alloys. *Metal. Sci.*, 8 pp. 117–124.

4. Bilde-Sorensen, J. B. 1983. Creep in particle-containing materials. *Deformation of Multi Phase and Particle Containing Materials*, Riso National Laboratory, Roskilde, Denmark.

5. Peterseim, J., and Sauthoff, G. 1983. Analysis of the dependence of creep on stress, temperature and on the distribution of small particles in Fe-Cr-alloys. *Deformation of Multi Phase and Particle Containing Materials*, Riso National Laboratory, Roskilde, Denmark.

6. Caron, S., and Masounare, J. 1990. A literature review on fabrication techniques of particulates reinforced metal composites. *Fabrication of Particulates Reinforced Metal Composites*, ASM International, Materials Park, Ohio.

7. Lugscheider, E., AH-Mekideche, A., and Melzer, A. 1994. Verbasserung der eigenschaften von hartlegierungen durch auftraggeschweisste carbidische verbundpulver. *Schweissen and Schneiden*, 46 (3): 34–37.

8. Cola, M. J., Lienert, T. J., Gould, J. E., and Hurley, J. P. 1990. Laser welding of a SiC particulate reinforced aluminum metal matrix composite. *Proc. of ASM Weldability of Materials Symposium*, Detroit, Mich., October 6–12, pp. 297–303, ASM International, Materials Park, Ohio.

9. Altshiuller, B., Christy, W., and Wiskel, B. 1990. GMA welding of Al-Al_2O_3 metal matrix composite. *Proc. of ASM Weldability of Materials Symposium*, Detroit, Mich., October 6–12, pp. 305–309, ASM International, Materials Park, Ohio.

10. Ahearn, J. S., Cooke, C., and Fishman, S. F. 1982. Fusion welding of SiC reinforced Al composites. *Metal Const.* 14 (4): 192–197.

11. Lundin, C. D., Danko, J. C., and Swindeman, C. J. 1989. Fusion welding of SiC reinforced aluminum alloy 2024. *2nd Intn. Conf. on Trends in Welding Research*, Gatlinburg, Tenn., pp. 303–307, ASM International, Materials Park, Ohio.

12. Thomas, R. D. 1978. The effect of ferrite on the creep rupture properties of austenitic weld metals. *Welding Journal* 57: 81-s to 86-s.

13. Evans, R. W., and Wilshire, B. 1985. *Creep of Metals and Alloys*, The Institute of Metals, London, England.

14. Rohatgi, P., and Asthana, R. 1976. The solidification of metal-matrix particulate composites. *JOM* 43(5): 35–41.

15. Omenyi, S. N., and Neumann, A. W. 1976. Thermodynamic aspects of particle engulfment by solidifying melts. *J. Applied Physics* 47: 3956–3962.

16. Uhlmann, D. R., Chalmers, B., and Jackson, K. A. 1965. Interaction between particles and a solid-liquid interface. *J. Applied Physics* 25: 2986–2993.

17. Stefanescu, D. M., Dhindaw, B. K., Kacar, S. A., and Meitra, A. 1988. Behavior of ceramic particles at the solid-liquid metal interface in metal composites. *Met. Trans.*, 19A: 2847–2855.

18. Azbel, D., and Liapis, A. I. 1982. Motion of solid particles in a liquid medium. *Handbook of Fluids in Motion*, ed. N.P. Cheremisinoff and R. Gupta, Ann Arbor Science Publishers, Ann Arbor, Mich.

19. Lajoye, L., and Suery, M. 1988. Modelling of particle segregation during casting of Al-matrix composites. *Cast Reinforced Metal Composites*, ASM International, Metals Park Ohio.

20. *Handbook of Chemistry and Physics*. 64th Ed., 1983. CRC Press, Boca Raton, Fla.

21. Fee, A. R., Segabache, R., and Tobolski, E. L. 1987. Microhardness testing. *Metals Handbook*, Ninth Ed., Vol. 8, ASM International, Materials Park, Ohio.

22. Hench, L. L., and West, J. K. 1990. The sol-gel preparation. *Chem. Rev.* 90: 33–72.

23. Brownlee, J. K., Matlock, D. K., and Edwards, G. R. 1987. Effects of aluminum and titanium on the microstructure and properties of microalloyed steel weld metal. *Trends for Welding Research*, ed. by S. A. David, pp. 245-250, ASM International, Materials Park, Ohio.

24. Caulfield, T., Bellows , R. S., and Tien, J. K. 1985. Interdiffusional effect between tungsten fibers and an iron-nickel-base alloy. *Met. Trans.*, 16A: 1961–1968.

25. Orper, G. M., and Sickly, J. 1987. A comprehensive representation of transient weld pool development in spot welding operations. *Met. Trans.*, 18A: 1325–1332.

26. Woods. R. A., and Milner, D. R. 1971. Motion in the weld pool in arc welding. *Welding Journal*, 50: 163-s to 173-s .